JOURNAL OF THERMOPHYSICS AND HEAT TRANSFER
Vol. 24, No. 4, October–December 2010

# Computation of Vibration-Dissociation Nonequilibrium Boundary Layers: Comparison of Various Models

N. Belouaggadia*
*Hassan II University, 20800 Casablanca, Morocco*
I. Armenise†
*Istituto di Metodologie Inorganiche e dei Plasmi,*
*Consiglio Nazionale delle Ricerche, 70126 Bari, Italy*
M. Capitelli‡
*Bari University, 70126 Bari, Italy*
F. Esposito§
*Istituto di Metodologie Inorganiche e dei Plasmi,*
*Consiglio Nazionale delle Ricerche, 70126 Bari, Italy*
and
R. Brun¶
*Université de Provence, 13170 Les Pennes Mirabeau, France*

DOI: 10.2514/1.46520

**In the inner part of the dissociated boundary layer of hypersonic bodies, a vibrational freezing zone has been observed. This freezing region takes place even if, in the outer part of the boundary layer, translation and vibration temperatures are in equilibrium and even if the surface is catalytic. This phenomenon can be attributed to the diffusion towards the wall of the vibrational energy; consequently the dissociation rate constants in this region can increase. Advanced physical models taking into account the vibration-chemistry interaction are required for the description of such flows. State-to-state and statistical global models are described in this paper and used in the computation of hypersonic boundary layers. All methods can predict the general features of the freezing phenomenon and present a qualitative agreement, as far as similar assumptions are used. Applications to boundary layers behind a reflected shock wave and along a hemispherical body are also presented.**

## Nomenclature

| | | |
|---|---|---|
| $A$ | = | chemical symbol |
| $C$ | = | $\rho\mu/\rho_e\mu_e$ |
| $C_f$ | = | frozen specific heat, J kg$^{-1}$ K$^{-1}$ |
| $c_i$, $c_p$ | = | $\rho_i/\rho$, $\rho_p/\rho$ |
| $c_v$ | = | vibrational specific heat, J kg$^{-1}$ K$^{-1}$ |
| $Ec$ | = | Eckert number |
| $e$ | = | total internal energy (per unit mass), J kg$^{-1}$ |
| $e_v$ | = | vibrational energy, J kg$^{-1}$ |
| $\dot{e}_v$ | = | vibrational energy source term (inelastic collisions), W m$^{-3}$ |
| $f'$ | = | $u/u_e$ |
| $f$ | = | distribution function, m$^{-6}$ s$^3$ |
| $g$ | = | $h_0/h_{0e}$ |
| $h$ | = | enthalpy (per unit mass), J kg$^{-1}$ |
| $i$, $j$, $k$, $l$ | = | vibrational levels |
| $J$ | = | collisional term (Boltzmann equation), m$^{-6}$ s$^2$ |
| $K$ | = | reaction rate constant, s$^{-1}$ |
| $Le$, $Le_v$ | = | Lewis number, vibrational Lewis number |
| $m$ | = | elementary mass, kg |
| $\mathbf{P}$ | = | stress tensor |
| $Pr$ | = | Prandtl number |
| $p$ | = | pressure, Pa |
| $Q$ | = | quantity $Q$ in equilibrium |
| $q$ | = | heat flux, Wm$^{-2}$ |
| $R$ | = | gas constant, J kg$^{-1}$ K$^{-1}$ |
| $\boldsymbol{r}$ | = | generalized spatial coordinate |
| $r$ | = | transverse coordinate, m |
| $S$ | = | source term |
| $Sc$ | = | Schmidt number |
| $T$ | = | translation-rotation temperature, K |
| $t$ | = | time, s |
| $\boldsymbol{U}$ | = | diffusion velocity, m s$^{-1}$ |
| $u$ | = | longitudinal component of $\boldsymbol{V}$, m s$^{-1}$ |
| $\boldsymbol{u}$ | = | peculiar velocity, m s$^{-1}$ |
| $\boldsymbol{V}$ | = | macroscopic velocity, m s$^{-1}$ |
| $\dot{w}$ | = | mass source term, kg m$^{-3}$ s$^{-1}$ |
| $X$ | = | molar concentration, m$^{-3}$ |
| $x$, $y$ | = | intrinsic coordinates, m |
| $z_p$ | = | $c_p/c_{pe}$ |
| $\beta$ | = | $\mathrm{d}u_e/\mathrm{d}x$, s$^{-1}$ |
| $\gamma$ | = | recombination coefficient at the wall |
| $\theta$ | = | $T/T_e$ |
| $\partial$ | = | partial derivative |
| $\varepsilon_p$ | = | $e_{vp}/e_{vpe}$ |
| $\vartheta$ | = | reference time |
| $\mu$ | = | viscosity, kg m$^{-1}$ s$^{-1}$ |
| $\nu$ | = | stoichiometric coefficient |
| $\xi$, $\eta$ | = | Lees–Levy–Dorodnitsin transformation coordinates |
| $\rho$ | = | density, kg m$^{-3}$ |
| $\varphi$ | = | first-order perturbation of the distribution function |

Received 28 July 2009; revision received 3 May 2010; accepted for publication 6 May 2010. 

*Associate Professor, Mohamedia, Faculté des Sciences Ben M'Sik, Département de Physique, Avenue Cdt, Driss el harti B.P: 7955-Ben M'Sik; aya_walid@menara.ma.

†Researcher, Via Amendola 122/D; iole.armenise@ba.imip.cnr.it.

‡Full Professor, Chemistry Department, Istituto di Metodologie Inorganiche e dei Plasmi, Consiglio Nazionale delle Ricerche, Via Orabona 4; mario.capitelli@ba.imip.cnr.it. Associate Fellow AIAA.

§Researcher, Via Amendola 122/D; fabrizio.esposito@ba.imip.cnr.it.

¶Professor Emeritus, 42 Chemin des Petits Cadeneaux; brun-raymond@orange.fr.

$\tau$ = relaxation time, s
$\psi$ = Von Mises transverse coordinate

*Subscripts*

$b$ = backward reaction
$c$ = chemistry
$d$ = dissociation
$e$ = outer edge of the boundary layer
$f$ = forward reaction, frozen condition
$i, j, k, l$ = vibrational quantum levels
$p$ = reaction product
$p, q$ = molecular species $p$, atomic species $q$
$r$ = rotation, reactant
$s$ = chemical reaction
$t$ = translation
$v$ = vibration
$w$ = wall condition
0 = stagnation condition

## I. Introduction

IN HIGH stagnation enthalpy flows, the boundary layers around various bodies may be simultaneously in strong vibrational and chemical nonequilibrium. This is the case in the intermediate hypersonic regime corresponding to conditions characteristic of flows around reentry bodies for which the stagnation enthalpies range from 5 to 15 MJ/Kg.

In the inner part of these boundary layers, a vibrational freezing zone has been observed [1,2], that is the vibrational population and consequently the vibration energy remains at a much higher level than their equilibrium value, so that, close to the body, where the translational temperature is strongly decreasing, the dissociation rate constants may increase. This freezing region takes place even if, in the outer part of the boundary layer, translational and vibrational temperatures are in equilibrium and even if the wall may be considered as catalytic [3]. Without dissociation, such a freezing region has also been observed [4].

This phenomenon can be attributed to the diffusion towards the wall of the vibrational energy which has a characteristic diffusion rate much higher than the deexcitation rate due to the decreasing translational temperature: this may be easily deduced from the dimensionless form of the macroscopic conservation and relaxation equations. The consequence of this behavior is that the dissociation rate constants can increase in this nonequilibrium region despite the decrease of the translational temperature and, in any case, remain higher than their Arrhenius equilibrium values. The phenomenon of course is amplified by a possible noncatalytic property for the vibration at the wall, as has been experimentally shown [5,6].

It is therefore obvious that advanced physical models taking into account the vibration-chemistry interaction are required for the description of such flows. Thus, in the recent past, several state-to state models have been developed and used especially for the analysis of the stagnation region of blunt bodies [7–10], where the flow quantities vary strongly and are at the origin of these nonequilibrium phenomena. These models treat the vibrational states (or rotational-vibrational states) as particular species and the corresponding balance equations for vibrational populations take into account all possible transitions including dissociation, recombination and chemical reactions. Detailed features of the flow can then be described by this way. On the other hand, global models including vibration-chemistry interaction have also been used [7,11].

The essential purpose of this paper is to compare state-to-state models recently developed in [12,13] and a global statistical model presented and developed in [14,15] and based on the application of a generalized Chapman–Enskog procedure. The second aim of the paper is to show that these models give a correct description of the boundary-layer flows and present a relatively good agreement in their common domain of validity, for example for the determination of dissociation rate constants.

First, the general equations of hypersonic flow in vibrational and chemical nonequilibrium are presented, pointing out the main parameters characterizing this type of flow and requiring a specific modelling such as the chemical and vibrational source terms. Then the equations of the boundary layer close to the stagnation point are developed as a typical and important example; a general presentation of the state-to-state (STS) models and the global (GM) model used to solve these equations is also proposed and the results obtained by these different methods are also analyzed for a dissociating pure gas and a reactive mixture (air). Thus, the results obtained with the various models show that the freezing phenomenon, the increase of the dissociation rate constants close to the wall and the role of the wall catalycity are correctly predicted by the presented methods. A qualitative agreement is generally observed between the results given by these methods, especially for the rate constants. Specific results are also presented, such as the profiles of vibrational populations across the stagnation point boundary layer computed with STS methods and the evolution of the vibrational nonequilibrium and dissociation rate constants in an unsteady boundary layer computed with the global model.

## II. General Equations

### A. Mathematical Symbols and Notations

Scalar symbols are in italic, vectorial symbols in bold italic and tensorial ones in bold block capital. Dotted symbols are used for chemical source terms. The contracted product of $\mathbf{ab}$ is $\mathbf{a}.\mathbf{b}$ and the double contracted product of $\mathbf{AB}$ is $\mathbf{A}:\mathbf{B}$. $\frac{\partial}{\partial \boldsymbol{r}}$ is the symbolic vector with $\frac{\partial}{\partial x}, \frac{\partial}{\partial y}, \frac{\partial}{\partial z}$ as Cartesian components. The derivations with a prime (such as $f'$) are with respect to the variable $\eta$ defined by Eq. (9).

### B. Conservation Equations

We consider high enthalpy flows in the intermediate hypersonic regime, that is flows composed of molecules and atoms in vibrational and chemical nonequilibrium. The Boltzmann equations for each molecular species $p$ and each atomic species $q$ may be written in the following respective forms:

$$\frac{\mathrm{d}f_{ip}}{\mathrm{d}t} = J_{trp} + J_{vp} + J_{cp} \tag{1}$$

$$\frac{\mathrm{d}f_{q}}{\mathrm{d}t} = J_{tq} + J_{cq} \tag{2}$$

where the collisional terms $J$ have been split into three or two parts: $J_t$ includes the TT (translation-translation) exchanges (elastic collisions), $J_{tr}$ includes the TR (translation-rotation) exchanges, $J_v$ the vibrational exchanges and $J_c$ the chemical exchanges corresponding to dissociation, recombination and exchange reactions. We assume $\tau_{tr} \ll \tau_v$, $\tau_c$ and $\tau_v < \tau_c$ (nitrogen for example) or $\tau_v \sim \tau_c$ (oxygen for example).

Multiplying Eqs. (1) and (2) by the general collisional invariants (mass, momentum, energy), integrating over the velocity space, summing over the rotational and vibrational levels and adding the corresponding equations, we obtain the three usual global conservation equations for mass, momentum and energy governing the mixture:

$$\frac{\partial \rho}{\partial t} + \frac{\partial . \rho \boldsymbol{V}}{\partial \boldsymbol{r}} = 0 \tag{3}$$

$$\rho \frac{\mathrm{d}\boldsymbol{V}}{\mathrm{d}t} = -\frac{\partial . \mathbf{P}}{\partial \boldsymbol{r}} \tag{4}$$

$$\rho \frac{\mathrm{d}e}{\mathrm{d}t} = -\frac{\partial . \boldsymbol{q}}{\partial \boldsymbol{r}} - \mathbf{P}: \frac{\partial \boldsymbol{V}}{\partial \boldsymbol{r}} \tag{5}$$

where $\rho$, $\boldsymbol{V}$, $e$, $\mathbf{P}$, $\boldsymbol{q}$, respectively, represent the density, velocity, total energy, stress tensor, and heat flux of the mixture. However, in the present case of vibrational and chemical nonequilibrium, it is also necessary to know the evolution of the vibrational energy $e_V$ and the

concentration of species $\rho_p/\rho$. Equations (3–5), therefore must be completed by vibrational relaxation equations (for molecular species $p$) and by species conservation equations ($p$ and $q$). These last equations differ if we consider a global (statistical) model or state-to-state models.

For the global model, we consider only one single relaxation equation for each species $p$ involving the global vibrational energy. This equation is obtained by multiplying Eq. (1) by $\varepsilon_{ip}$, integrating and summing over all levels. Thus, we have

$$\rho_p \frac{\mathrm{d}e_{vp}}{\mathrm{d}t} + \frac{\partial.\boldsymbol{q}_{vp}}{\partial \boldsymbol{r}} = \dot{e}_{vp} + \dot{w}_{vp} \tag{6}$$

where $\dot{e}_{vp}$ is the vibrational energy production term due to nonreactive collisions (vibration exchange, or TV, and vibration–vibration exchange, or VV) and $\dot{w}_{vp}$ the production term due to reactive collisions (the dotted symbol means total derivative with respect to time).

In the same way, we need species conservation equations which are obtained by multiplying Eqs. (1) and (2) by $m_p$ and $m_q$, respectively, integrating and summing over levels. Thus, for example, we obtain for species $p$

$$\frac{\partial \rho_p}{\partial t} + \frac{\partial.\rho_p \boldsymbol{V}_p}{\partial \boldsymbol{r}} = \dot{w}_p \tag{7}$$

where $\boldsymbol{V}_p = \boldsymbol{V} + \boldsymbol{U}_p$ and where $\dot{w}_p$ represents the mass source term for species $p$ due to chemical reactions.

In the state-to-state models, the population of each vibrational level is considered as a particular species, so that we have the following equation for the density of species $ip$

$$\frac{\partial \rho_{ip}}{\partial t} + \frac{\partial.\rho_{ip} \boldsymbol{V}_{ip}}{\partial \boldsymbol{r}} = \dot{w}_{ip} \tag{8}$$

where $\dot{w}_{ip}$ is the source term from all types of reactions including vibrational exchanges. For atomic species, we have equations similar to Eq. (7).

The problem is now to close this equation system, that is to propose expressions for the source terms $\dot{e}_{vp}$, $\dot{w}_{vp}$, $\dot{w}_{ip}$ and $\dot{w}_p$ and also for the transport terms $\mathbf{P}$, $\boldsymbol{q}$, $\boldsymbol{q}_{vp}$ and $\boldsymbol{V}_p$. This is the aim of the physical models described hereafter. However, before presenting these models, we develop the boundary-layer equations governing the hypersonic flow close to bodies where dissipative and nonequilibrium effects are particularly important.

### C. Boundary-Layer Equations

Considering axisymmetric steady flows in vibrational and chemical nonequilibrium, we apply the usual Lees–Levy–Dorodnitsin (LLD) transformation $(x, y) \to (\xi, \eta)$ to the previous conservation equations, i.e.

$$\xi = \int_0^x \rho_e \mu_e u_e r^2 \,\mathrm{d}x, \qquad \eta = \frac{\rho_e u_e r}{\sqrt{2\xi}} \int_0^y \frac{\rho}{\rho_e} \,\mathrm{d}y \tag{9}$$

so that, with the usual boundary-layer approximations, we obtain the following equations for the general momentum, energy, and species Eqs. (4), (5), and (7), respectively

$$(Cf'')' + ff'' + \frac{2\xi}{u_e}\frac{\mathrm{d}u_e}{\mathrm{d}\xi}\left(\frac{\rho_e}{\rho} - f'^2\right) = 2\xi\left(f'\frac{\partial f'}{\partial \xi} - f''\frac{\partial f}{\partial \xi}\right) \tag{10}$$

$$\left(\frac{C}{Pr}g'\right)' + fg' + Ec_e\left[\left(1-\frac{1}{Pr}\right)Cf'f''\right]' + \left[\frac{C}{Sc}\left(\frac{1}{Le}-1\right)\sum_p \frac{h_{pe}c_{pe}}{h_{0e}}z'_p\right]' = 2\xi\left(f'\frac{\partial g}{\partial \xi} - g'\frac{\partial f}{\partial \xi}\right) \tag{11}$$

$$\left(\frac{C}{Sc}z'_p\right)' + fz'_p - \frac{2\xi}{c_{pe}}\left(f'z_p\frac{\mathrm{d}c_{pe}}{\mathrm{d}\xi} - \frac{\dot{w}_p}{\rho\rho_e\mu_e u_e^2 r^2}\right) = 2\xi\left(f'\frac{\partial z_p}{\partial \xi} - z'_p\frac{\partial f}{\partial \xi}\right) \tag{12}$$

where the new unknowns are $f' = u/u_e$, $g = h_0/h_{0e}$ and $z_p = c_p/c_{pe}$ and where the partial derivations (indicated with a prime) are with respect to $\eta$.

Now, for the global model, the vibrational relaxation Eq. (6) becomes

$$\left(\frac{C}{Sc}\varepsilon_p z'_p\right)' + \frac{1}{c_{pe}}\left(\frac{C}{ScLe_v}\varepsilon'_p\right)' + fz_p\varepsilon'_p - \frac{2\xi}{e_{vpe}}\left(f'\varepsilon_p\frac{\mathrm{d}e_{vpe}}{\mathrm{d}\xi} - \frac{\dot{w}_{vp} - e_{vpe}\varepsilon_p\dot{w}_p}{\rho\rho_{pe}\mu_e u_e^2 r^2}\right) = 2\xi\left(f'\frac{\partial \varepsilon_p}{\partial \xi} - \varepsilon'_p\frac{\partial f}{\partial \xi}\right) \tag{13}$$

where $\varepsilon_p = e_{vp}/e_{vpe}$ and where the derivations are also with respect to $\eta$.

In these equations, Navier–Stokes expressions for $\mathbf{P}$, $\boldsymbol{q}$, $\boldsymbol{q}_v$, $\boldsymbol{V}_p$ are used, corresponding to the first order Chapman–Enskog expansion for the distribution functions. In the same way, nondimensional expressions for the transport terms are used ($C, Pr, Le, Sc, Ec$).

In the STS models, as each vibrational level of molecular species is considered as a different species, we can write the continuity equation for each species mass concentration in the following way

$$\left(\frac{C}{Sc}c'_{ip}\right)' + fc'_{ip} + \frac{2\xi}{\rho\rho_e\mu_e u_e^2 r^2}\dot{w}_{ip} = 2\xi\left(f'\frac{\partial c_{ip}}{\partial \xi} - c'_{ip}\frac{\partial f}{\partial \xi}\right) \tag{14}$$

where $c_{ip} = \rho_{ip}/\rho$ and where the derivations are also with respect to $\eta$. Moreover, each atomic species is considered as one single species.

### D. Boundary Layer Close to a Stagnation Point

The knowledge of the flow in this region is of obvious interest particularly for heat transfer problems. It is well known that, in this case, self-similar solutions for the previous Eqs. (10–14), exist because at the stagnation point, we have

$$x = \xi = 0, \qquad u_e = 0, \qquad \frac{\mathrm{d}u_e}{\mathrm{d}x} = \beta, \qquad \frac{2\xi}{u_e}\frac{\mathrm{d}u_e}{\mathrm{d}\xi} = \frac{1}{2}, \qquad r \sim x$$

so that the momentum and the species equations may be, respectively, written

$$(Cf'')' + ff'' + \frac{1}{2}\left(\frac{\rho_e}{\rho} - f'^2\right) = 0 \tag{15}$$

$$\left(\frac{C}{Sc}z'_p\right)' + fz'_p + \frac{1}{2}\frac{\dot{w}_p}{\rho\beta c_{pe}} = 0 \tag{16}$$

In the case of global models, the transformed equations for total energy and vibrational energy, deduced from Eqs. (11) and (13) are, respectively, the following:

$$\left(\frac{C}{Pr}g'\right)' + fg' + \left[\frac{C}{Sc}\left(\frac{1}{Le}-1\right)\sum_p \frac{h_{pe}c_{pe}}{h_{0e}}z'_p\right]' = 0 \tag{17}$$

$$\left(\frac{C}{Sc}\varepsilon_p z'_p\right)' + \frac{1}{c_{pe}}\left(\frac{C}{ScLe_v}\varepsilon_p\right)' + fz_p\varepsilon'_p + \frac{1}{2}\frac{\dot{w}_{vp} - e_{vp}\dot{w}_p}{\rho\beta e_{vpe}c_{pe}} = 0 \tag{18}$$

In the case of STS models, the Eqs. (16) and (18) are replaced by the following ones, deduced from Eqs. (14)

$$\left(\frac{C}{Sc}c'_{ip}\right)' + fc'_{ip} + \frac{1}{2}\frac{\dot{w}_{ip}}{\rho\beta} = 0 \tag{19}$$

The source terms $\dot{w}_{ip}$ are due to VV, VTm (VT molecule–molecule collision), VTa (VT atom-molecule collision), dissociation, recombination, and exchange processes.

These equations may be further simplified if we assume constant values for the dimensionless numbers throughout the boundary layer. Thus, in the stagnation point boundary layer (Sec IV.A), $Pr$, $Sc$, $Le$, $Le_v$ are assumed constant in all methods. As $C$ may significantly vary in the boundary layer, it is considered as dependent of $T$ [16] in the global model; in the STS model, however, it is assumed constant.

The boundary conditions are the following. As $\eta \to \infty$ (outside of the boundary layer): $f' \to 1$, $g \to 1$, $z_p \to 1$, $\varepsilon_p \to 1$, $c_{ip} \to \rho_{ipe}/\rho_e$ and the physical quantities correspond to the inviscid stagnation conditions (equilibrium, Sec. IV.A). For $\eta = 0$ (wall): $f = f' = 0$ and $T = T_w$ (=Constant). The value of the other quantities depend on the assumed catalytic properties of the wall. Thus, for catalytic conditions, species concentrations and vibrational energy take their equilibrium value at $T = T_w$. For noncatalytic conditions, their normal derivatives are zero. For partially catalytic conditions, the recombination process is proportional to the diffusion flux of atoms toward the wall.

## III. Physical Models

### A. Global Model

As discussed above, the problem consists in finding expressions for the source terms $\dot{e}_{vp}$, $\dot{w}_p$ and $\dot{w}_{vp}$. The determination of $\dot{e}_{vp}$ may be simply carried out by using the harmonic oscillator model including TV and VV exchanges between various species. Details and explicit expressions are available in [14,15,17]. The determination of $\dot{w}_p$ and $\dot{w}_{vp}$ must be deduced from the set of $s$ chemical reactions taking place in the reactive mixture considered, that is

$$\sum_{\mathrm{p}} \nu'_{ps} A_p \underset{\leftarrow}{\overset{\rightarrow}{}} \sum_{\mathrm{p}} \nu''_{ps} A_p \tag{20}$$

Considering the forward and backward reactions $f$ and $b$, respectively, we have

$$\dot{w}_p = \sum_s (\dot{w}_{pfs} - \dot{w}_{pbs}) = \sum_s M_p (\nu''_{ps} - \nu'_{ps}) (K_{fs} \Pi_p X_p^{\nu'_{ps}} - K_{bs} \Pi_p X_p^{\nu''_{ps}}) \tag{21}$$

and

$$\dot{w}_{vp} = \sum_s [(e_{vp} - e_{vpfs}) \dot{w}_{pfs} - (e_{vp} - e_{vpbs}) \dot{w}_{pbs}] \tag{22}$$

We now have to determine the rate constants $K_{fs}$ and $K_{bs}$ and also the vibrational energies gained or lost in chemical reactions $s$, i.e. $e_{vpfs}$ and $e_{vpbs}$. These quantities depend on the vibrational nonequilibrium and may be obtained from a generalized Chapman–Enskog (GCE) procedure.

Thus, expanding the distribution functions in a series of the assumed small parameter $\tau_v/\vartheta$ and truncating the expansion at the first order, we have to solve the following system instead of the full Boltzmann equation

$$J^0_{trvp} = 0 \tag{23}$$

$$\frac{\mathrm{d}f^0_{ip}}{\mathrm{d}t} = J^1_{trvp} + J^0_{cp} + J^1_{cp} \tag{24}$$

Details on the method used to solve this system may be found in [18]. The first-order solution obtained for $f_{ip}$, that is $f^1_{ip} = f^0_{ip}(1 + \varphi_{ip})$ is thus valid in vibrational and chemical nonequilibrium zones up to complete equilibrium; i.e., it takes into account the TRV nonequilibrium which is at the origin of the transport terms as well as the interaction vibration-chemistry.

Thus, explicit relations for the reaction rate constants are obtained and they may be expressed as functions of the vibrational nonequilibrium [14]. For example, we find for the dissociation rate constants $K_d$

$$K_d = \bar{K}_d \left(1 + \frac{e_v - \bar{e}_v}{RT} \frac{e_{vd} - \bar{e}_v}{\bar{e}_v}\right) \tag{25}$$

where $\bar{K}_d$ is the Arrhenius rate constant and $e_{vd}$ the vibrational energy lost due to the dissociation. We have similar relations for the recombination and exchange reactions. In the same way, given the first-order solution for $f_{ip}$, we find expressions for $e_{vd}$ from its definition

$$e_{vd} = \frac{\sum_{i_v} \int_{\boldsymbol{u}} J_d e_{i_v} \, \mathrm{d}\boldsymbol{u}}{\sum_{i_v} \int_{\boldsymbol{u}} J_d \, \mathrm{d}\boldsymbol{u}} \tag{26}$$

For each reaction (forward, backward), we can thus determine the loss (or gain) for vibrational energy of the involved component $p$, i.e., $e_{vfps}$ and $e_{vbps}$. For example, at the zero order of the distribution function, we find a value for $e_{vd}$ close to $0.5e_d$ with the harmonic oscillator model and close to $0.4e_d$ with the anharmonic model depending slightly on the species. At the first order of the distribution function, the expressions are more complex but an approximate value of $0.3e_d$ is used, in agreement with other determinations [15]. Thus, the vibration-dissociation coupling appears in the expressions of the rate constants involving molecular species and in vibrational relaxation Eq. (6). However, the model is not capable of taking into account the influence of the nonequilibrium on the recombination rates involving only atomic species so that, for the corresponding reactions we assume $K_r = \bar{K}_r$, but this is a commonly used assumption.

Comparisons with Park's two-temperature semiempirical model [19] taking also into account the vibration-dissociation coupling have been made for two cases. One is discussed in section 4.2.1. for the case of an unsteady boundary layer and another has been presented in [20], where shock detachment distances over hemispherical bodies have been computed by both methods and also compared with experimental results; it seems clear that the two-temperature model significantly underestimates these distances [7,20].

### B. STS Models

The STS models have been also developed for applications to the boundary layer of a stagnation point [2,21]; thus, hereafter, they are presented in the framework of this application.

As discussed above, in the STS models, the molecules in the different levels are treated as specific species [Eq. (19)]. Furthermore, starting from the energy equation written in terms of temperature rather than in terms of enthalpy, assuming constant values for the dimensionless numbers $Le$, $Sc$ and $Pr$ throughout the boundary layer and assuming $C = 1$, we can rewrite the energy equation in the following form

$$\theta'' + Prf\theta' = S_T \tag{27}$$

with $\theta = T/T_e$ and where $S_T$ depends on the balance of vibrational energy due to all reactions, i.e.

$$S_T = \frac{Le}{C_f T_e} \sum_p \sum_i (e_i^p S_i) \tag{28}$$

where the species $p$ are the molecular species of the mixture.

In the same way, we can rewrite the continuity Eq. (19) in the following form

$$c_i'' + Scfc_i' = S_i \tag{29}$$

where $S_i = -\frac{Sc\dot{w}_i}{2\rho\beta}$ represents the balance of the population of the $i$th species due to VV, VTa, VTm, dissociation, recombination and exchange processes and may be classically written in a way similar to Eq. (21), involving the concentrations of reactants (forward and backward reactions), the corresponding rate constants and stoichiometric coefficients, i.e.

$$S_i = -\sum_j B(i,j)c_j \tag{30}$$

with

$$B(i,j) = \frac{Sc}{\beta}\sum_s \left\{ \left[ \prod_k (\rho c_k)^{\nu^r_{ks}} \right] (\rho c_j)^{(\nu^r_{ks}-1)} \mathrm{sgn}(\nu^p_{is}) K_s \right\} \tag{31}$$

for $i \neq j$, and

$$B(i,i) = -\sum_l B(l,i) \tag{32}$$

for $i = j$, and $l \neq i$

Because of the difficulty in deriving the dissociation and recombination rate coefficients from experiments, they are derived from two main theoretical approaches: the ladder climbing (LC) model and the quasi-classical trajectory (QCT) model.

The dissociation-recombination process in the LC model [12] assumes that the created atoms are molecules in a vibrational level (named *pseudolevel*) just above the last bounded level and that the dissociation-recombination themselves are VV and VT processes involving this pseudolevel. The dissociation rates are calculated by extrapolating the VV and VT rates to the pseudolevel and the recombination rates are calculated by the detailed balance principle.

The quasi-classical trajectory (QCT) method is a molecular dynamics method used to calculate cross sections (and rate coefficients) of chemical kinetics processes. It reaches its aim thanks to the pseudoquantization of reactants and products and the classical evolution of the system. In particular, the $N_2 + N$ collisions rate coefficients by QCT, used in the present work, have been calculated taking into account all the possible outcomes of the collision process: nonreactive, reactive, dissociation, quasi-bound states. Moreover the cross sections from each initial rovibrational state towards each final vibrational state $w$ have been obtained summing contributions from any final rotational state compatible with $w$; then the rate coefficients from a given vibrational state to each possible final vibrational state have been calculated averaging on a given rotational temperature, taken equal to the translational temperature. The calculations carried out with the QCT method enable us to determine not only the VT rates due to nitrogen atom-nitrogen molecule impact [13,22–24] but also the dissociation rates by nitrogen atom-nitrogen molecule impact. In the present work, the notation QCT indicates that the dissociation due to nitrogen atom-nitrogen molecule collisions is directly studied by using the QCT rates, whereas the dissociation due to molecule-molecule impact is still studied as an extension of the VV and VT molecule-molecule processes to the pseudolevel (LC model). The dissociation due to molecule-molecule impact is still investigated by means of the LC model due to the lack of data for the corresponding QCT rates. By analogy with the atom-molecule impact case (see Sec. IV.A.1), it is possible to estimate that the assumption of the LC model should underestimate the degree of nonequilibrium. It is interesting to note that quantum and semi-classical rates for both deactivation and dissociation rates for the system $N/N_2$ were recently investigated by a NASA group [25,26] using a more sophisticated Potential Energy Surface.

## IV. Applications, Results, Comparisons, and Discussion

### A. Boundary Layer Close to a Stagnation Point

The behavior of the hypersonic boundary layer close to a stagnation point is examined by solving the corresponding Eqs. (15–19) for the case of a dissociating pure gas ($N_2$) and a reactive mixture (air) and with boundary conditions given in Sec. II.C. Moreover, the following stagnation conditions have been chosen:

$$T_{0e} = 6000 \text{ K}, \qquad T_w = 1000 \text{ K}, \qquad \beta = 5 \cdot 10^3 \text{ s}^{-1}$$

A few computations have also been made for a stagnation temperature of 7000 K without changing the other parameters.

These values correspond to reentry conditions corresponding to a Mach number of about 23. Nondimensional transport terms $(Pr, Le, Sc)$ are assumed constant through the boundary layer, with $Pr = 0.71$, $Le = 1.45$ for both methods, so that $Sc = 0.49$. In the global model, $Le_v = 1$, [16], and chemical rate constants (Arrhenius) and vibrational relaxation times of $N_2$ and $O_2$ are deduced from the harmonic oscillator and Schwartz–Slavski–Herzfeld (SSH) models and are taken from usual references [27,28]. NO, as usual, is considered to be in vibrational equilibrium. Thus, in the global model, 17 chemical reactions are considered, of which 15 are dissociation-recombination reactions for $N_2$, $O_2$ and NO and 2 are exchange reactions involving NO.

In the STS models, VV, VTm, VTa, dissociation-recombination kinetic processes $N_2 + N_2, N_2 + N$ are taken into account in the case of the pure gas ($N_2$), and also processes $O_2 + O_2, O_2 + O, N_2 + O$, $NO + N$ in the case of air. The dissociation rate constants (pseudofirst-order dissociation constants) are easily defined from individual rate constants. Thus, for example, in the case of the $N_2/N$ mixture, we have for $K_d$

$$K_d N_{\text{tot}} = \sum_i K^{i_{\max}\to i_{\max}+1}_{i\to i-1} \mathrm{N_2}(i_{\max})\mathrm{N_2}(i) + K^{VTm}_{i_{\max}\to i_{\max}+1}\mathrm{N_2}(i_{\max})\mathrm{N_2} + \sum_i K^{VTa}_{i\to i_{\max}+1}\mathrm{N_2}(i)\mathrm{N} \tag{33}$$

for the LC model, and

$$K_d N_{\text{tot}} = \sum_i K^{i_{\max}\to i_{\max}+1}_{i\to i-1} \mathrm{N_2}(i_{\max})\mathrm{N_2}(i) + K^{VTm}_{i_{\max}\to i_{\max}+1}\mathrm{N_2}(i_{\max})\mathrm{N_2} + \sum_i K^{d}_{i}\mathrm{N_2}(i)\mathrm{N} \tag{34}$$

for the QCT model.

Similar formulas may be written for the components of air. In this case 118 species are considered in the STS models: 68 for $N_2$ (one for each $N_2$ vibrational level), 47 for $O_2$ (one for each $O_2$ vibrational level), 1 for N, 1 for O and 1 for NO, indeed the NO molecule is assumed in vibrational equilibrium. The vibrational energies are calculated with the semiclassical WKB (Wentzel-Kramers-Brillouin) method. Catalytic and noncatalytic cases are considered.

#### 1. *Case of a Pure Gas*

*a. Vibrational Distributions: STS Methods.* Considering the case of dissociating nitrogen, the vibrational distributions through the boundary layer are obtained from STS methods and are represented in Figs. 1 and 2. A strong nonequilibrium distribution may be observed particularly close to the wall, so that in the inner part of the boundary layer a vibrational frozen zone ($e_v > \bar{e}_v$) does exist; this nonequilibrium is accentuated by the noncatalycity of the wall, as this may be observed by comparing Figs. 1a and 2a or 1b and 2b.

In the noncatalytic case, the dissociation rate of the reaction $N_2 + N$ computed by the QCT model leads to a much stronger vibrational nonequilibrium (Fig. 1a) than that calculated by LCM (Fig. 1b), particularly in the inner zone of the boundary layer, whereas the LCM distribution tends to equilibrium in the outer zone. These important differences observed between both methods become smaller if the vibrational ladder is cut at $v_{\max} = 60$ instead of 68. Details may be found in [13], however, a short discussion is needed here. Different from the LC model where the dissociation rates are just derived from the extrapolation of the VT rates, in the QCT calculations the dissociation could affect the VT relaxation of the last bound levels. Therefore the VTa rate coefficients toward the level $v = 60$ are closer, although always lower, to the QCT dissociation rates than the VTa rate coefficients towards the level $v = 67$. It follows that cutting the vibrational ladder to $v_{\max} = 60$ causes the QCT model to behave more similarly to the LC model. To conclude, the LC model, extrapolating the VT rates in the continuum, strongly underestimates the dynamical results.

When the surface is partially catalytic ($\gamma = 5.10^{-2}$), the distributions are not too affected by the model (Figs. 2a and 2b): the strong nonequilibrium developed close to the wall, essentially due to the surface recombination, suddenly drops in the boundary layer with the

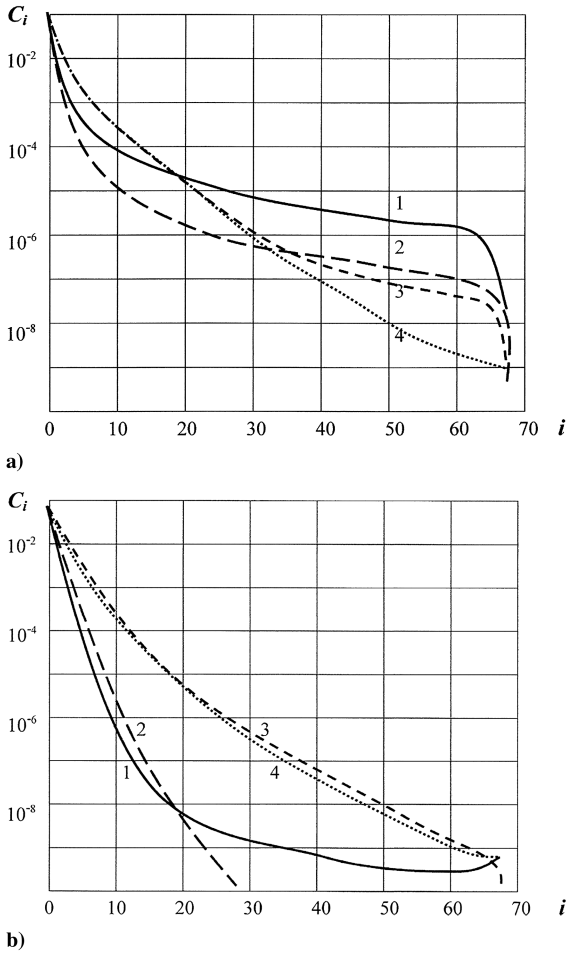


**Fig. 1 Nitrogen vibrational distributions in the boundary layer: a) QCT model, noncatalytic wall, and b) LC model, noncatalytic wall. Line 1, $\eta = 0$ (wall), line 2, $\eta = 1$, line 3, $\eta = 4$, and line 4, $\eta = 8$.**

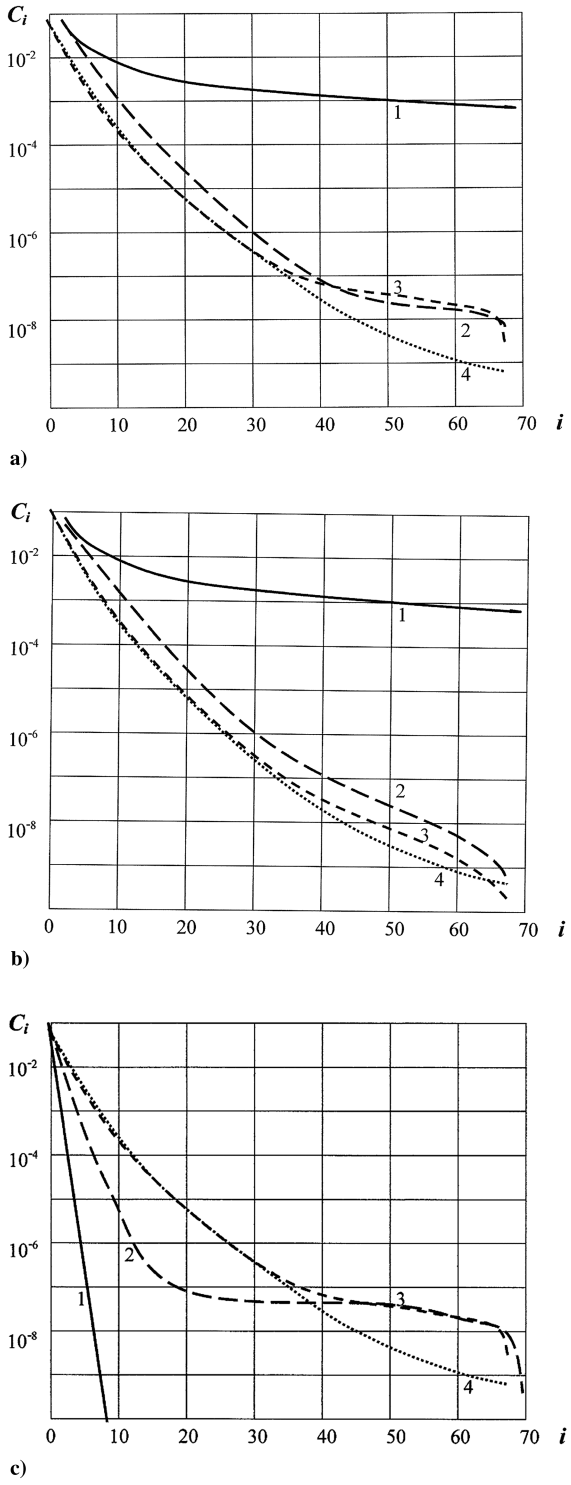


**Fig. 2 Nitrogen vibrational distributions in the boundary layer: a) QCT model, partially catalytic wall, b) LC model, partially catalytic wall, and c) QCT model, fully catalytic wall. Line 1, $\eta = 0$ (wall), line 2, $\eta = 1$, line 3, $\eta = 4$, and line 4, $\eta = 8$.**

exception of the distribution tails for which the nonequilibrium is more important in the QCT model case (Fig. 2a).

In the fully catalytic case, in the very neighborhood of the wall ($\eta = 0$) the distribution is close to equilibrium because the surface is catalytic for both chemistry and vibration, whereas in the rest of the boundary layer a strong nonequilibrium prevails quite comparable to the noncatalytic case (Fig. 2c).

However, if we assume no gas-phase reactions, the vibrational population progressively passes from equilibrium at the boundary-layer edge to a strong nonequilibrium close to the surface (Fig. 3), this phenomenon being due to diffusion processes as discussed in the introduction.

*b. Macroscopic Parameters: Rate Constants.* Comparisons may be made between global and STS methods for the macroscopic parameters, temperatures, concentrations and rate constants. The strong overpopulation of the high levels close to the wall leads to a strong nonArrhenius behavior of the dissociation rate constants in this region. Thus, we observe an increase of $K_d$ when approaching the wall, despite the temperature decrease. Note that this behavior is provided by all methods, STS and global ones, as shown in Figs. 4 and 5 for noncatalytic and catalytic cases, respectively. A similar effect was found in the case of a pure $O_2/O$ mixture [29]; in that case the LC model was used for the gas-phase dissociation. In Figs. 4 and 5, we also observe that the values given by LCM are much lower than those deduced from QCT and global models which are in qualitative agreement. If, however, in the LCM, the vibrational ladder is stopped at $v_{\max} = 60$, the difference is much smaller, as it is the case for the vibrational distribution (Fig. 4).

For the fully catalytic case, $K_d$ remains higher than $\bar{K}_d$ but does not increase when approaching the wall and suddenly drops very close to the wall as expected (Fig. 4b). A consequence of these results is an increase of the molecular concentration when approaching the wall, for both catalytic and noncatalytic cases. This increase, of course, is much more important in the catalytic case because of the strong recombination and is observed for all physical models (Fig. 6).

An effective vibrational temperature $T_V$ may be deduced from previous computations. Thus in the STS model this temperature is defined as the vibrational temperature related to the first two vibrational levels. In the global model, this temperature is defined by assuming that the computed value of $e_v$ is the equilibrium (Boltzmann) value corresponding at this temperature, but with the

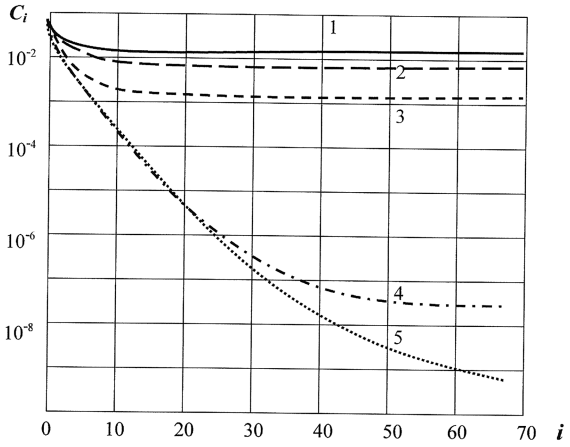


**Fig. 3 Nitrogen vibrational distributions in the boundary layer (no gas-phase kinetics, partially catalytic wall). Line 1, $\eta = 0$ (wall), line 2, $\eta = 1$, line 3, $\eta = 4$, line 4, $\eta = 7.90$, and line 5, $\eta = 8$.**

harmonic oscillator model, used here, these definitions are identical. We find that the difference of the vibrational temperatures $T_V$ given by STS and global models, is not very important, as shown in Fig. 7, with the values for $T_V$ at the wall of 4180, 4040, and 4070 K for the QCT, LCM, and global models, respectively. Similarly, the computations performed for $T_{0e} = 7000$ K give corresponding values of 4600, 4200, and 4300 K.

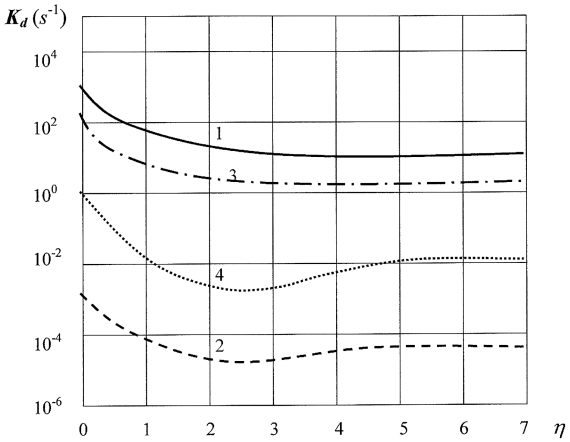


a)

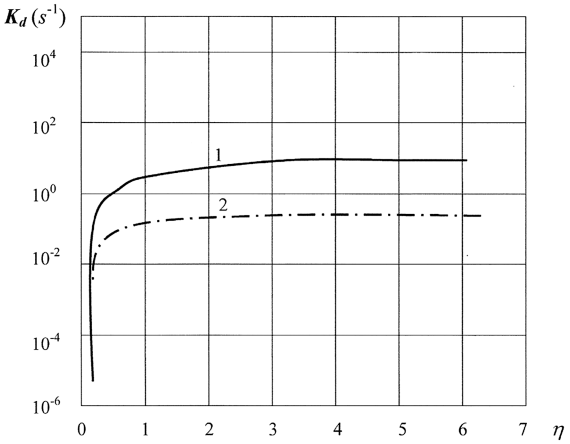


b)

**Fig. 4 Nitrogen dissociation rate constants across the boundary layer: a) noncatalytic wall, with line 1 indicating the QCT model, line 2 the LC model, line 3 the global model, and line 4 the LC model ($i_{\max} = 60$), and b) fully catalytic wall, with line 1 indicating the QCT model, and line 2 the global model.**

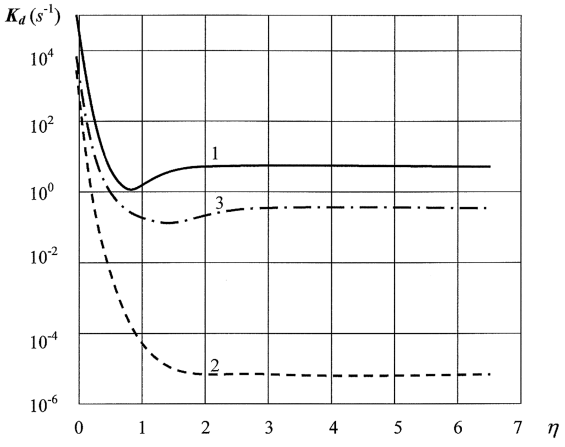


**Fig. 5 Nitrogen dissociation rate constants across the boundary layer (partially catalytic wall), with line 1 indicating the QCT model, line 2 the LC model, and line 3 the global model.**

*2. Case of Mixtures*

The boundary-layer equations have also been solved using a $N_2$, N, $O_2$, O and NO mixture simulating air at high temperature, with the same conditions as above with the $N_2$/N case. The physical models used are the QCT and global models and the wall is considered as noncatalytic for chemistry.

We observe that, whereas the distribution of $N_2$ is roughly similar to the distribution for pure $N_2$ (Fig. 1a), the distribution of $O_2$ is practically frozen through the boundary layer and is closer to an equilibrium distribution (Fig. 8). This is due of course to faster relaxation in the case of $O_2$.

This may be also observed in the spatial profiles of vibrational temperatures throughout the boundary layer (Fig. 9). The values of $T_V$ themselves, given by both methods, QCT and global are in relatively good agreement, as seen in the same figure. We also obtain comparable values for $N_2$, $O_2$, NO dissociation rate constants deduced from both methods and, in particular, we observe a strong non-Arrhenius behavior close to the wall (Fig. 10).

### B. Boundary Layer Behind a Reflected Shock

To give another example of a boundary layer in vibration-dissociation nonequilibrium, an unsteady boundary layer behind a reflected shock wave is analyzed below with the global model. The scheme of the flow is represented in Fig. 11. The equations of the one-dimensional unsteady boundary layer developing along the end-wall, written in $(y, t)$ physical coordinates are transformed in the $(\psi, \tilde{t})$ plane with the Von Mises transformation [similar to the LLD transformation, Eq. (9)]

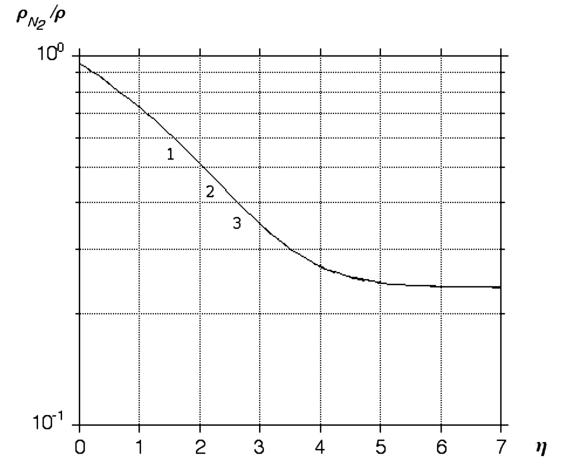


**Fig. 6 Nitrogen mass fractions across the boundary layer (partially catalytic wall), with line 1 indicating the QCT model, line 2 the LC model, and line 3 the global model.**

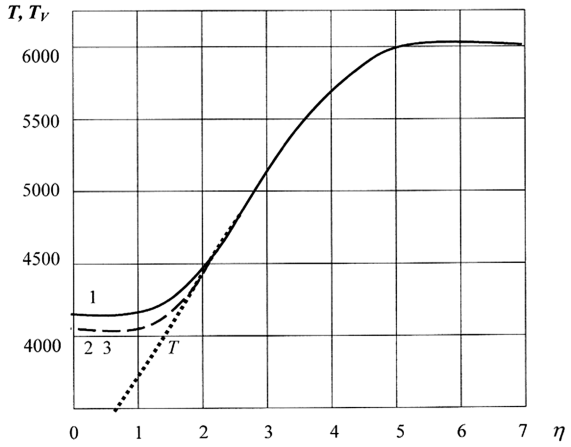


**Fig. 7 Nitrogen vibrational temperatures across the boundary layer (noncatalytic wall), with line 1 indicating the QCT model, line 2 the LC model, and line 3 the global model.**

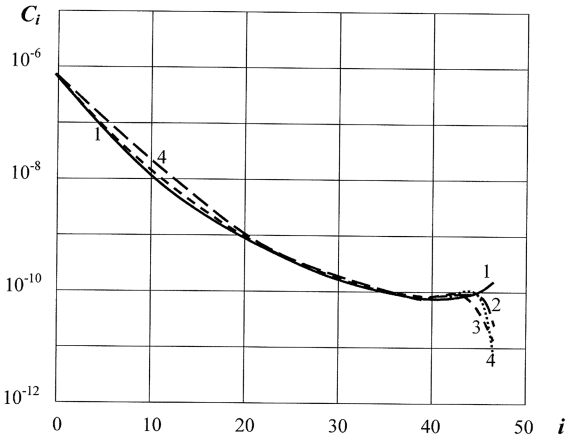


**Fig. 8 Oxygen vibrational distributions in the boundary layer (QCT model, noncatalytic wall). Line 1, $\eta = 0$ (wall), line 2, $\eta = 1$, line 3, $\eta = 4$, and line 4, $\eta = 8$.**

$$\tilde{t} = \int_0^t \rho_e \mu_e \, \mathrm{d}t, \qquad \psi = \frac{1}{\sqrt{2\tilde{t}}} \int_0^y \rho \, \mathrm{d}y \tag{35}$$

Computations are made for nitrogen as a test gas with initial pressure and temperature of 200 Pa and 295 K, respectively, and for an incident shock Mach number of 12, so that the flow is in

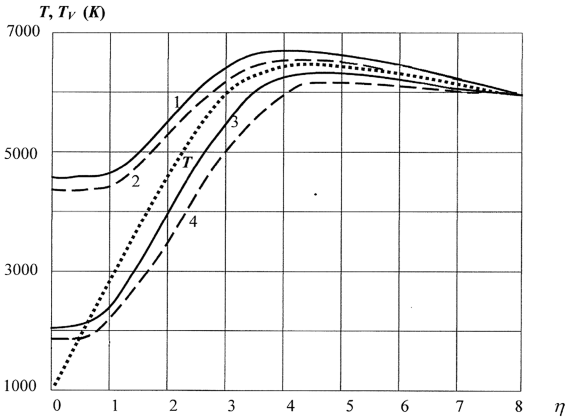


**Fig. 9 Nitrogen and oxygen vibrational temperatures across the boundary layer (noncatalytic wall). Line 1, $N_2$, QCT model; line 2, $N_2$, global model; line 3, $O_2$, QCT model; and line 4, $O_2$, global model.**

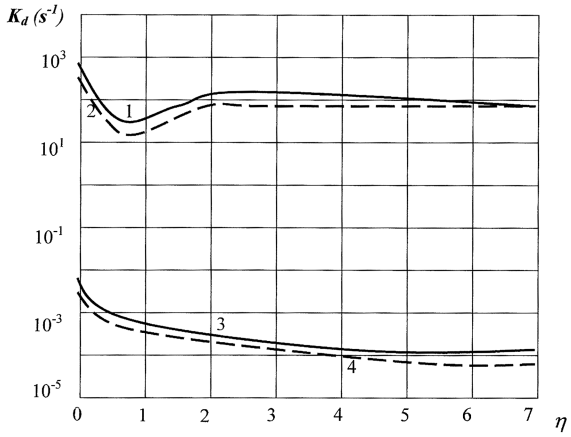


**Fig. 10 Nitrogen and oxygen dissociation rate constants across the boundary layer (noncatalytic wall). Line 1, $N_2$, QCT model; line 2, $N_2$, global model; line 3, $O_2$, QCT model; and line 4, $O_2$, global model.**

vibrational and chemical nonequilibrium behind the incident and reflected shock waves.

The details of the flow may be found in [3] and here the main interest of the analysis lies in the behavior of the vibrational nonequilibrium across the boundary layer. To that end, in Fig. 12, spatial profiles of the dimensionless vibrational energy nonequilibrium $(\bar{e}_v - e_v)/\bar{e}_{ve}$ are represented for successive times after the reflection and with a wall ($\psi = 0$) assumed either fully catalytic or noncatalytic for the vibration and the chemistry.

Considering first the catalytic case, during the first stages of the relaxation following the reflection the vibrational nonequilibrium decreases monotonously from the outer flow to the wall, as expected (curve A). For subsequent times, a minimum (with a negative value) appears in the profiles (curve B), attaining a constant value when the outer flow is in equilibrium (curve C). Thus, as previously, two regions may be distinguished in the boundary layer: an outer zone where $T > T_V$, as usual behind a shock wave, and an inner zone where $T < T_V$, corresponding to a freezing zone and due to the diffusion of vibrational energy towards colder regions close to the wall, where the relaxation time becomes longer.

This result has consequences for the dissociation rate constants, and for example, we have $K_D > \bar{K}_D$ in the inner region. When the wall is considered as catalytic, the curve representing $K_D$ presents a maximum (Fig. 13). In the noncatalytic case, the vibrational nonequilibrium and the dissociation rate constants continue to increase up to the wall (Figs. 12 and 13), accentuating the non-Arrhenius character of these rate constants. Also in Fig. 13, values for $K_d$ obtained from the two-temperature model [19] are presented, showing a similar behavior.

Finally, to generalize the results obtained in the boundary layer of a stagnation point, complete Navier–Stokes equations including the present global model are solved around an hemispherical body. As in the previous examples, a vibrational nonequilibrium zone is found

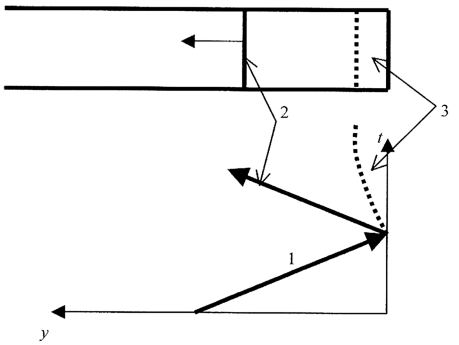


**Fig. 11 Scheme of boundary layer developing at the end-wall of a shock tube (physical plane and $y$, $t$ diagram). Line 1, incident shock, line 2, reflected shock, and line 3, boundary layer.**

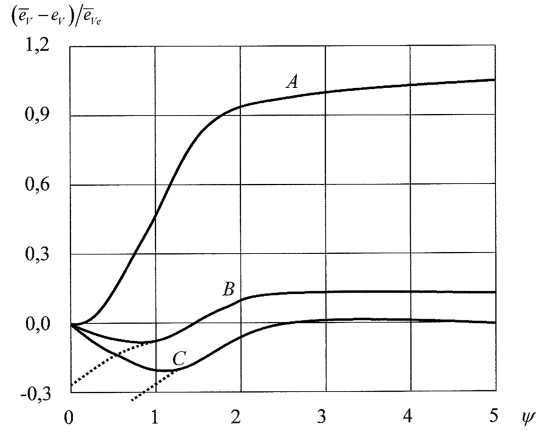


**Fig. 12 Vibrational nonequilibrium distribution across the boundary layer: time after reflection. Line A, 25 $\mu$s, line B, 500 $\mu$s, line C, 900 $\mu$s. Solid line is catalytic wall, and dotted line is noncatalytic wall.**

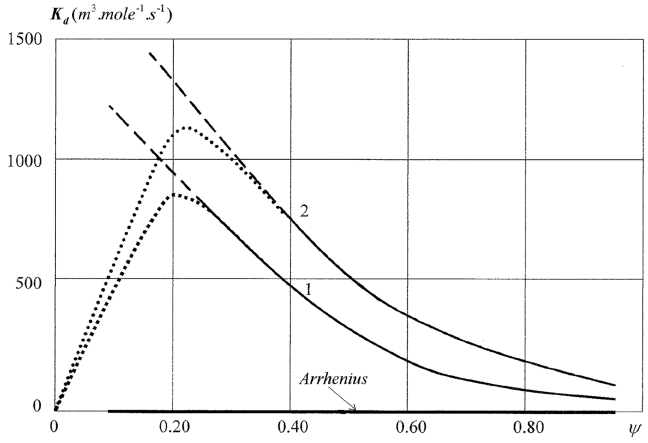


**Fig. 13 Dissociation rate constant close to the wall. Line 1: present global model: solid line is common part, dashed line is noncatalytic, and dotted line is catalytic. Line 2: Park's model: solid line is common part, dashed line is noncatalytic, and dotted line is catalytic.**

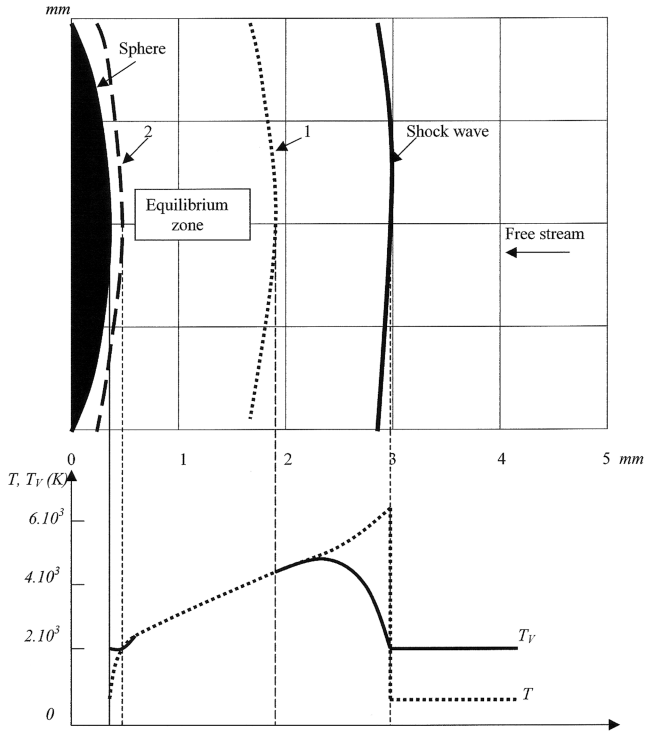


**Fig. 14 Hypersonic nitrogen flow over an hemispherical body (lines 1 and 2: $T = T_V$ curves).**

close to the wall developing along the body in the expansion part of the flow. The upper part of Fig. 14 shows an example of the scheme of the flow-field over an hemispherical body ($R = 2$ cm) placed in a hypersonic nitrogen flow of a shock tunnel [20] ($M_\infty = 7.25$, $T_\infty = 420$ K, $T_{V\infty} = 2000$ K). The lower part of Fig. 14 represents the spatial profiles of temperatures along the stagnation line, summarizing the results presented in Sec. IV.A.

## V. Conclusions

Different methods of analysis of nonequilibrium reacting boundary layers have been presented including STS and global physical models. Applications and comparisons have been made, mainly in the case of the boundary layer of a stagnation point, but also for other types of boundary layers. In all cases, vibrational nonequilibrium zones have been observed close to the body wall. These zones are essentially due to the diffusion of vibrational energy and they are amplified by the noncatalytic character of the walls. The consequence is a corresponding increase of the dissociation rate constants, which in turn affects the wall heat transfer. A qualitative agreement between results given by various methods has been observed in the general behavior of these phenomena, and this may be considered as reasonable when taking into account the various uncertainties and assumptions included in each model. However, better quantitative agreement is expected from further future studies.

## Acknowledgments

The present paper has been partially supported by Agenzia Spaziale Italiana under the Configurazioni Aerotermodinamiche Innovative per Sistemi di Trasporto spaziale project.

## References

[1] Armenise, I., Capitelli, M., and Gorse, C., "Nitrogen Nonequilibrium Vibrational Distributions and Non-Arrhenius Dissociation Constants in Hypersonic Boundary Layers," *Journal of Thermophysics and Heat Transfer*, Vol. 12, No. 1, 1998, pp. 45–51. doi:10.2514/2.6300

[2] Armenise, I., Capitelli, M., and Gorse, C., "State-to-State Approach in the Kinetics of Air Components Under Re-Entry Conditions," *Journal of Thermophysics and Heat Transfer*, Vol. 11, No. 4, 1997, pp. 570–578. doi:10.2514/2.6281

[3] Belouaggadia, N., Brun, R., and Takayama, K., "Characteristics Features of Boundary Layers in Vibration-Dissociation Non-Equilibrium," *Shock Waves*, Vol. 16, No. 1, 2006, pp. 17–23. doi:10.1007/s00193-006-0045-y

[4] Brun, R., Duran, G., Philippi, P. C., Dourrieu, M. F., and Tosello, R., "Linearized Kinetic Models for Polyatomic Gases and Mixtures of Gases: Application to Vibrationally Relaxing Flows," In *Flames, Lasers and Reactive Systems*, edited by J. R. Bowen, N. Manson, A. K. Oppenheim and R. I. Soloukin, Vol. 304, Progress in Aeronautics and Astronautics, AIAA, New York, 1983, p. 293.

[5] Brun, R., Moustaghfir, A. K., and Meolans, G., "Gas-Wall Interaction in Vibrational Non-Equilibrium Flows," *Shock Waves, Proceedings of the 21st International Symposium on Shock Waves*, Paper 1621, Univ. of Queensland, New South Wales, Australia, 1997.

[6] Brun, R., Guibergia, J. P., and Marmey, R., "Influence de la Relaxation de Vibration sur la Couche Limite à L'Aval d'Une Onde de Choc Mobile," *Comptes Rendus de l'Académie des Sciences*, Vol. 268, No. 166, 1969, pp. 166–169.

[7] Josyula, E., and Bailey, W. F., "Vibration-Dissociation Coupling Using Master Equations in Non-Equilibrium Hypersonic Blunt-Body Flow," *Journal of Thermophysics and Heat Transfer*, Vol. 15, No. 2, 2001, pp. 157–167. doi:10.2514/2.6604

[8] Josyula, E., Bailey, W. F., and Ruffin, S., "Reactive and Non-Reactive Vibrational Energy Exchanges in Non-Equilibrium Hypersonic Flows," *Physics of Fluids*, Vol. 15, No. 10, 2003, pp. 3223–3235. doi:10.1063/1.1608013

[9] Orsini, A., Rini, P., Taviani, V., Fletcher, D., Kustova, E. V., and Nagnibeda, E. A., "State-to-State Simulation of Non-Equilibrium Nitrogen Stagnation Line Flows: Fluid Dynamics and Vibrational Kinetics," *Journal of Thermophysics and Heat Transfer*, Vol. 22, No. 3, 2008, pp. 390–398.

doi:10.2514/1.34545
[10] Kustova, E., Nagnibeda, E., Armenise, I., and Capitelli, M., "Non-Equilibrium Kinetics and Heat transfer in $O_2/O$ Mixtures near Catalytic Surfaces," *Journal of Thermophysics and Heat Transfer*, Vol. 16, No. 2, 2002, pp. 238–244.
doi:10.2514/2.6673
[11] Candler, G. V., Olejniczak, J., and Harrold, B., "Detailed Simulation of Nitrogen Dissociation in Stagnation Regions," *Physics of Fluids*, Vol. 9, No. 7, 1997, pp. 2108–2117.
doi:10.1063/1.869330
[12] Armenise, I., Capitelli, M., and Gorse, C., "Fundamental Aspects of the Coupling of Non-Equilibrium Vibrational Kinetics and Dissociation-Recombination Processes with the Boundary Layer Fluid Dynamics in N2 and Air Hypersonic Flows," *Molecular Physics and Hypersonic Flows*, edited by M. Capitelli, Vol. 482, NATO-ASI Series C: Mathematical and Physical Sciences, Kluwer Academic, Norwell, MA, 1996, pp. 703–716.
[13] Armenise, I., Esposito, F., and Capitelli, M., "Dissociation-Recombination Models in Hypersonic Boundary Layer Flows," *Chemical Physics*, Vol. 336, No. 1, 2007, pp. 83–90.
doi:10.1016/j.chemphys.2007.05.015
[14] Belouaggadia, N., and Brun, R., "Chemical Rate Constants in Non-Equilibrium Flows," *Journal of Thermophysics and Heat Transfer*, Vol. 12, No. 4, 1998, pp. 482–488.
doi:10.2514/2.6393
[15] Belouaggadia, N., and Brun, R., "Statistical Model for Vibration-Chemical Reaction Interaction: Extension to Gas Mixtures," *Journal of Thermophysics and Heat Transfer*, Vol. 20, No. 1, 2006, pp. 148–150.
doi:10.2514/1.14426
[16] Pascal, S., and Brun, R., "Transport Properties in Non-Equilibrium Gas Mixtures," *Physical Review E (Statistical Physics, Plasmas, Fluids, and Related Interdisciplinary Topics)*, Vol. 47, No. 5, 1993, pp. 3251–3267.
doi:10.1103/PhysRevE.47.3251
[17] Belouaggadia, N., Olivier, H., and Brun, R., "Numerical and Theoretical Study of the Shock Stand-Off Distance in Non-Equilibrium Flows," *Journal of Fluid Mechanics*, Vol. 607, No. , 2008, pp. 167–197.
doi:10.1017/S0022112008001973
[18] Brun, R., *Introduction to Reactive Gas Dynamics*, Oxford Univ. Press, New York, 2009.
[19] Park, C., "Assessment of Two-Temperature Kinetic Model for Dissociating and Weakly Ionized Nitrogen," *Journal of Thermophysics and Heat Transfer*, Vol. 2, No. 1, 1988, pp. 8–16.
doi:10.2514/3.55
[20] Belouaggadia, N., Hashimoto, T., Nonaka, S., Takayama, K., and Brun, R., "Shock Detachment Distance on Blunt Bodies in Non-Equilibrium Flow," *AIAA Journal*, Vol. 45, No. 6, 2007, pp. 1424–1429.
doi:10.2514/1.17806
[21] Doroshenko, V. M., Koudriavtsev, N. M., Novikov, S. S., and Smetanin, V. V., "Dependence of Heat Transfer on the Formation of Vibrationally Excited Nitrogen Molecules During the Recombination of Atoms in a Boundary Layer," *High Temperature*, Vol. 28, No. 1, 1990, pp. 70–76.
[22] Esposito, F., and Capitelli, M., "QCT Calculations for the Process $N_2(v) + N = N_2(v') + N$ in the Whole Vibrational Range," *Chemical Physics Letters*, Vol. 418, Nos. 4–6, 2006, pp. 581–585.
doi:10.1016/j.cplett.2005.11.036
[23] Esposito, F., Armenise, I., and Capitelli, M., "N-$N_2$ State-to-State Vibrational Relaxation and Dissociation Rates Based on Quasi-Classical Calculations," *Chemical Physics*, Vol. 331, No. 1, 2006, pp. 1–8.
doi:10.1016/j.chemphys.2006.09.035
[24] Esposito, F., Armenise, I., Capitta, G., and Capitelli, M., "O-$O_2$ State-to-State Vibrational Relaxation and Dissociation Rates Based on Quasi-Classical Calculations," *Chemical Physics*, Vol. 351, Nos. 1–3, 2008, pp. 91–98.
doi:10.1016/j.chemphys.2008.04.004
[25] Jaffe, R., Schwenke, D., Chaban, G., and Huo, W., "Vibrational and Rotational Excitation and Relaxation of Nitrogen from Accurate Theoretical Calculations," AIAA Paper No 2008-1208, Jan. 2008.
[26] Jaffe, R., Schwenke, D., and Chaban, G., "Theoretical Analysis of $N_2$ Collisional Dissociation and Rotation-Vibration Energy Transfer," AIAA Paper No 2009-1569, Jan. 2009.
[27] Millikan, R. C., and White, D. R., "Systematics of Vibrational Relaxation," *Journal of Chemical Physics*, Vol. 39, No. 12, 1963, pp. 3209–3213.
doi:10.1063/1.1734182
[28] Park, C., "A Review of Reaction Rates in High Temperature Air," AIAA Paper No 89-1740, June 1989.
[29] Kustova, E., Nagnibeda, E., Armenise, I., and Capitelli, M., "Nonequilibrium Kinetics and Heat Transfer in $O_2/O$ Mixtures near Catalytic Surfaces," *Journal of Thermophysics and Heat Transfer*, Vol. 16, No. 2, 2002, pp. 238–244.
doi:10.2514/2.6673